The tumor suppressor Lgl1 regulates NMII-A cellular distribution and focal adhesion morphology to optimize cell migration

Inbal Dahan, Ahuv Yearim*, Yarin Touboul, and Shoshana Ravid
Department of Biochemistry and Molecular Biology, Institute of Medical Research Israel-Canada, Hebrew University-Hadassah Medical School, Jerusalem 91120, Israel

ABSTRACT **The *Drosophila* tumor suppressor Lethal (2) giant larvae (Lgl) regulates the apical–basal polarity in epithelia and asymmetric cell division. However, little is known about the role of Lgl in cell polarity in migrating cells. In this study we show direct physiological interactions between the mammalian homologue of Lgl (Lgl1) and the nonmuscle myosin II isoform A (NMII-A). We demonstrate that Lgl1 and NMII-A form a complex in vivo and provide data that Lgl1 inhibits NMII-A filament assembly in vitro. Furthermore, depletion of Lgl1 results in the unexpected presence of NMII-A in the cell leading edge, a region that is not usually occupied by this protein, suggesting that Lgl1 regulates the cellular localization of NMII-A. Finally, we show that depletion of Lgl1 affects the size and number of focal adhesions, as well as cell polarity, membrane dynamics, and the rate of migrating cells. Collectively these findings indicate that Lgl1 regulates the polarity of migrating cells by controlling the assembly state of NMII-A, its cellular localization, and focal adhesion assembly.**

Monitoring Editor
Carole Parent
National Institutes of Health

Received: Jan 6, 2011
Revised: Dec 9, 2011
Accepted: Dec 20, 2011

INTRODUCTION

The establishment and maintenance of cell polarity are crucial for a diverse range of biological processes, including cell migration, asymmetric cell division, and epithelial apical–basal cell polarity. Cell polarity during cell migration is important to distinguish random cell migration, in which cells migrate in all directions in a noncoordinated manner, from directed cell migration, in which cells respond to polarizing cues to migrate in a given direction. In both cases, cell polarity is required to generate a front–rear axis (for review see Ridley *et al.*, 2003). The gene product of *Drosophila* Lethal (2) giant larvae (Lgl) is essential for the development of polarized epithelia and for cell polarity associated with asymmetric cell division of neuroblasts during fly development (Bilder *et al.*, 2000; Bilder and Perrimon, 2000; Ohshiro *et al.*, 2000; Peng *et al.*, 2000). Lgl is composed of two domains. The N-terminal region folds into two β-propellers, a structure that provides a docking platform for simultaneous interactions with multiple proteins. The C-terminal domain is an Lgl family-specific domain with unknown function (for review see Vasioukhin, 2006). Mammals have two Lgl homologues, Lgl1 and Lgl2. Lgl1 message is almost ubiquitously expressed, and Lgl2 is expressed in a tissue-specific manner and is necessary for proper placental development (Klezovitch *et al.*, 2004; Sripathy *et al.*, 2011). Loss of Lgl1 in mice results in formation of neuroepithelial rosette-like structures, similar to the neuroblastic rosettes in human primitive neuroectodermal tumors. Newborn Lgl1-knockout mice develop severe hydrocephalus and die neonatally (Klezovitch *et al.*, 2004). In addition, the expression of Lgl1 is strongly reduced in several tumor cell lines (Schimanski *et al.*, 2005; Kuphal *et al.*, 2006). Lgl1 is phosphorylated by atypical protein kinase C isoform ζ (aPKCζ), and this phosphorylation is important for the correct polarization in embryonic fibroblasts in response to wounding (Plant *et al.*, 2003) and for centrosome reorientation in astrocytes (Etienne-Manneville, 2008).

Biochemical and genetic analyses suggest that the *Drosophila* Lgl is the component of the cytoskeleton that interacts with nonmuscle myosin II (NMII), and this interaction is regulated by the phosphorylation of Lgl (Strand *et al.*, 1994a, 1994b; Kalmes *et al.*,

This article was published online ahead of print in MBoC in Press (http://www.molbiolcell.org/cgi/doi/10.1091/mbc.E11-01-0015) on January 4, 2012.

*Present address: Department of Human Molecular Genetics and Biochemistry, Sackler Medical School, Tel Aviv University, Tel Aviv 69978, Israel.

Address correspondence to: Shoshana Ravid (shoshr@ekmd.huji.ac.il).

Abbreviations used: ACD, assembly-competent domain; aPKCζ, atypical protein kinase C isoformζ; cACD, complementary ACD; GFP, green fluorescent protein; Lgl, Lethal (2) giant larvae; Lgl1, mammalian homologue of Lgl; MBP, maltose-binding protein; NMII, nonmuscle myosin II; NMII-A, nonmuscle myosin II isoform A; NMII-A Rod, Rod fragment of NMII-A; PBS, phosphate-buffered saline; shRNA, small hairpin RNA.

© 2012 Dahan *et al.* This article is distributed by The American Society for Cell Biology under license from the author(s). Two months after publication it is available to the public under an Attribution–Noncommercial–Share Alike 3.0 Unported Creative Commons License (http://creativecommons.org/licenses/by-nc-sa/3.0).

"ASCB®," "The American Society for Cell Biology®," and "Molecular Biology of the Cell®" are registered trademarks of The American Society of Cell Biology.

1996; Betschinger *et al.*, 2005). NMII is an actin-based motor protein that is important for cell migration through its effects on adhesion, lamellar protrusion, rear retraction, and polarity (for reviews see Conti and Adelstein, 2008; Vicente-Manzanares *et al.*, 2009b). NMII is a hexamer composed of two heavy chains of ~200 kDa and two pairs of essential and regulatory light chains of 17 and 20 kDa (for reviews see Tan *et al.*, 1992; Bresnick, 1999). The heavy chains include the α-helical coiled-coil rod domain responsible for the assembly of NMII monomers into filaments, the functional structures required for NMII activity, and contain the phosphorylation sites for several kinases (Murakami *et al.*, 2000; Dulyaninova *et al.*, 2005; Even-Faitelson and Ravid, 2006; Rosenberg and Ravid, 2006; Ronen and Ravid, 2009). Mammalian cells express three different NMII isoforms—NMII-A, NMII-B, and NMII-C (Shohet *et al.*, 1989; Simons *et al.*, 1991; Golomb *et al.*, 2004). In migrating fibroblasts, the NMII isoforms play different roles in cell polarization. NMII-A is dynamic and assembles actomyosin bundles in protrusions, specifically mediating retraction of the trailing edge during migration. In contrast, NMII-B incorporates into preformed F-actin bundles and remains stationary, defining the center and rear of the migrating cell (for review see Vicente-Manzanares *et al.*, 2009b).

The role of Lgl1 in apical–basal cell polarity has been studied extensively; however little is known about its role in polarization of migrating cells. In this study, we show that Lgl1 interacts directly with NMII-A, inhibiting its filament assembly in vitro. We provide data that Lgl1 restricts NMII-A from the cell leading edge and regulates the morphology of focal adhesions. Finally, we show that Lgl1 is required for proper cell polarization of migrating cells.

RESULTS

Lgl1 interacts directly with NMII-A

Studies in *Drosophila* indicate that Lgl is associated with NMII (Strand *et al.*, 1994a, 1994b). To find out whether a similar interaction also occurs in mammalian cells, we tested whether mammalian Lgl1 interacts with NMII-A. For this purpose we transfected Cos-7 cells with constructs encoding for Lgl1 tagged with green fluorescent protein (GFP; GFP-Lgl1) and NMII-A tagged with mCherry (mCherry-NMII-A). As shown in Figure 1A in the two rightmost columns, Lgl1 coimmunoprecipitated with NMII-A, indicating that the two proteins interact in vivo. In contrast, NMII-A was not detected in GFP immunoprecipitated from Cos-7 cells lysates transfected with GFP only, indicating that the interaction between Lgl1 and NMII-A is specific. To provide additional evidence for this Lgl1–NMII-A association, a reciprocal experiment was performed. For this purpose endogenous NMII-A was immunoprecipitated from HEK293T cells transfected with GFP-Lgl1 and subjected to Western blot analysis using GFP antibodies. As shown in Figure 1A in the two leftmost columns, GFP-Lgl1 was detected in NMII-A immunoprecipitates, further indicating that the two proteins form a complex in vivo. To test whether this interaction is direct, we performed pull-down assays using recombinant Lgl1 and its N- and C-terminal domains fused to maltose-binding protein (MBP; Figure 2A) and C-terminal Rod fragment of NMII-A (Figure 2B, NMII-A Rod). It is apparent that NMII-A Rod interacted directly with MBP-Lgl1-C but not with MBP-Lgl1-N (Figure 1B). These results are in agreement with the previous finding that the *Drosophila* NMII-binding domain to Lgl resides within the 515 amino acids of the Lgl C-terminal domain (Betschinger *et al.*, 2005). Of interest, NMII-A Rod did not bind to full-length MBP-Lgl1 (Figure 1B). To test whether the absence of this binding was due to the expression of misfolded Lgl1, we examined the ability of MBP-Lgl1 to bind to NMII-A in cell extract obtained from the SW620 cell line that expresses endogenous NMII-A (Figure 1C).

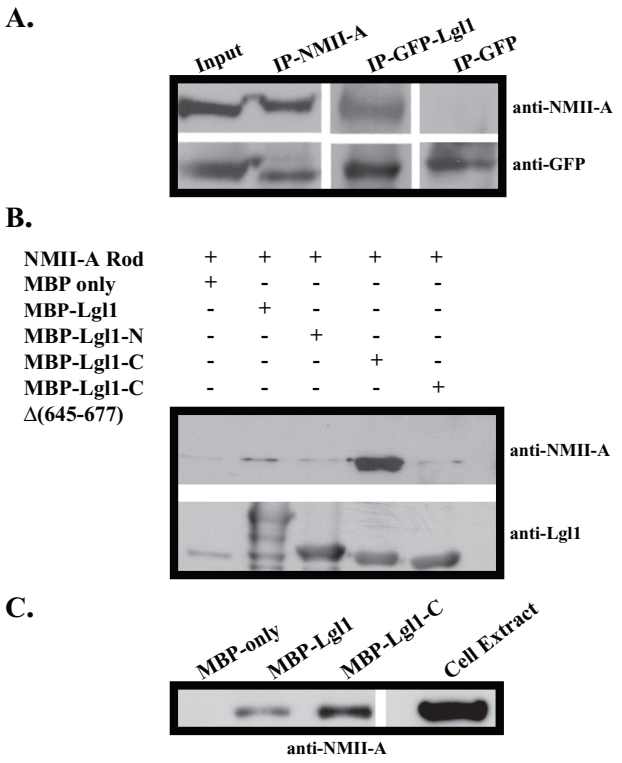

FIGURE 1: Lgl1 interacts directly with NMII-A. (A) Lgl1 coimmunoprecipitated with NMII-A. Cos-7 cells were cotransfected with GFP or GFP-Lgl1 and mCherry-NMII-A and subjected to immunoprecipitation using GFP-specific antibody (third and fourth lanes). For the reciprocal experiment, HEK293T cells were transfected with GFP-Lgl1 and subjected to immunoprecipitation with NMII-A antibody (second lane). The immunoprecipitated proteins were analyzed by immunoblotting with antibodies against NMII-A and GFP. (B) MBP-Lgl1-C coprecipitated with NMII-A Rod fragment in vitro. Lgl1 and its N- and C-terminal fragments fused to MBP were incubated with NMII-A Rod fragments and subjected to pull-down assay. The proteins were detected by immunoblotting with antibodies against NMII-A and Lgl1. MBP only was used as a negative control. (C) MBP-Lgl1 and MBP-Lgl1-C coprecipitated with NMII-A endogenously expressed by SW620 cells. MBP-Lgl1 and MBP-Lgl1-C were incubated with SW620 cell lysate and subjected to pull-down assay. The proteins were detected by immunoblotting with antibodies against NMII-A. MBP only was used as a negative control.

Both MBP-Lgl1 and MBP-Lgl1-C coprecipitate with NMII-A (Figure 1C), indicating that full-length MBP-Lgl1 can bind NMII-A in cell extract. We hypothesize that the bacterially expressed MBP-Lgl1 has a folded conformation, so its binding domain to NMII-A is not accessible. For this reason, in a pull-down assay using purified proteins, MBP-Lgl1 does not bind to NMII-A Rod. However, SW620 cells express a protein (or proteins) that unfolds the MBP-Lgl1. On addition of MBP-Lgl1 to SW620 cell extract, this protein binds to MBP-Lgl1, exposing its binding site to NMII-A and allowing the interaction between these two proteins. This hypothesis is supported by the findings that the *Drosophila* Lgl is found in an autoinhibited form in which the N-terminus interacts with the C-terminus, preventing it from binding to the cytoskeleton (Betschinger *et al.*, 2005).

Mapping of Lgl1 and NMII-A interacting domains

To define the region of Lgl1 that mediates its interactions with NMII-A, we generated a series of MBP-Lgl1-C terminal deletions

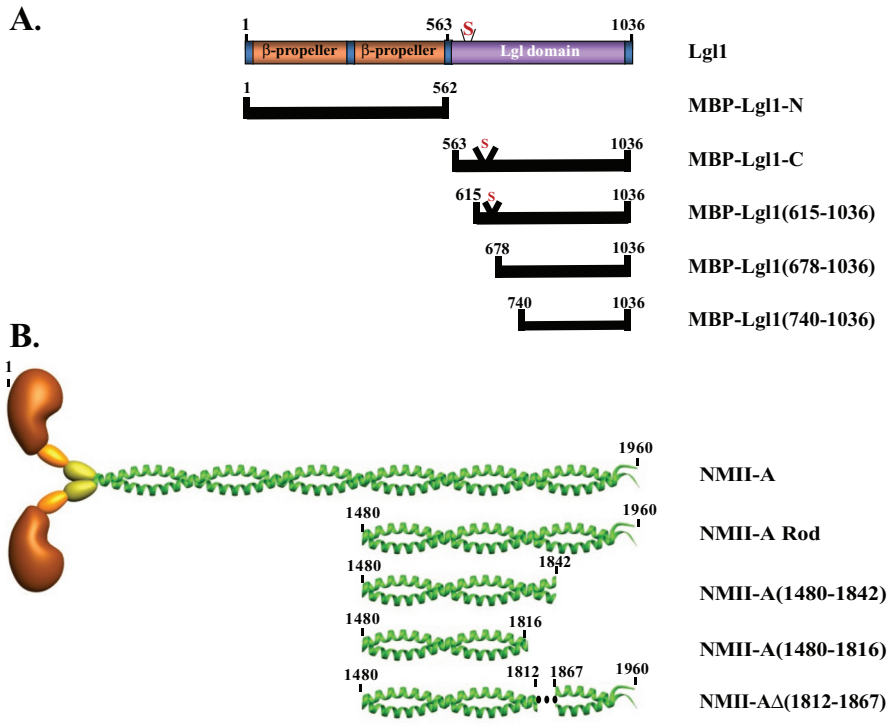

FIGURE 2: Schematic presentation of Lgl1 (A) and NMII-A (B) protein fragments used in this study. S, aPKCζ serine target sites. Numbers represent amino acid positions in the full-length proteins.

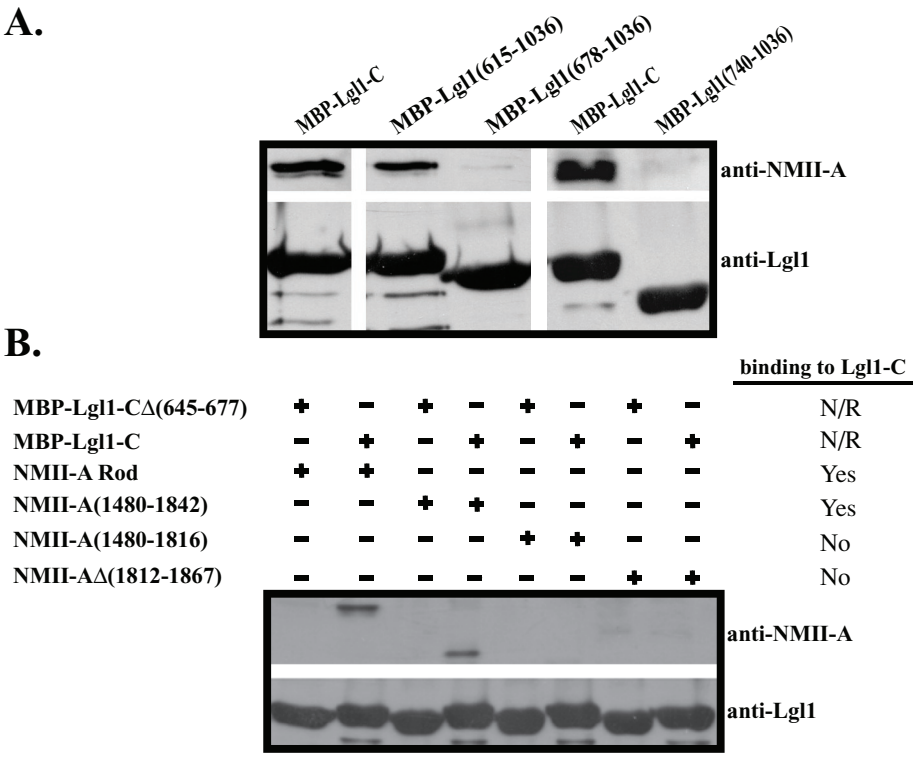

FIGURE 3: Mapping of Lgl1 and NMII-A interacting domains. (A) MBP-Lgl1-C fusion proteins with deletions at their N-terminal region were incubated with NMII-A Rod and subjected to pull-down assay. Proteins were detected by immunoblotting with antibodies against NMII-A and Lgl1. (B) NMII-A Rods containing deletions at their C-terminal were incubated with MBP-Lgl1-C or MBP-Lgl1-CΔ(645–677) as a negative control and subjected to pull-down assays. Proteins were detected by immunoblotting with antibodies against platelet NMII and Lgl1. N/R, not relevant.

(Figure 2A) and tested their ability to bind NMII-A Rod in pull-down assays (Figure 3A). Lgl1 containing residues 615–1036 (Figure 2A, Lgl1(615–1036)) bound to NMII-A Rod (Figure 3A), whereas Lgl1(678–1036) and Lgl1(740–1036) did not (Figure 3A). These findings indicate that Lgl1 binds to NMII-A Rod via residues 615–678. This region contains the five conserved serine residues that are phosphorylated by aPKCζ (Plant *et al.*, 2003), and phosphorylation of these sites in *Drosophila* Lgl leads to its dissociation from the cytoskeleton (Betschinger *et al.*, 2005). We therefore postulated that Lgl1 phosphorylation sites play a role in the interaction between Lgl1 and NMII-A. To test this hypothesis, we constructed MBP-Lgl1-C without the region containing the five conserved serine residues (MBP-Lgl1-C(645–677)) and tested its ability to bind NMII-A Rod. Indeed, this deletion completely abolished the binding of MBP-Lgl1-C to NMII-A Rod (Figures 1B and 3B). These results indicate that NMII-A interacts with Lgl1 via residues 645–677. These findings are in agreement with a previous report showing that addition of a peptide containing the five serine residues to *Drosophila* Lgl-NMII complex leads to the dissociation of the complex (Kalmes *et al.*, 1996).

To study the role of Lgl1 binding to NMII-A, we mapped the Lgl1-interacting domain to NMII-A. For this purpose we made a series of NMII-A Rod deletions at its C-terminal region (Figure 2B). These Rods were incubated with MBP-Lgl1-C fragment, and the mixture was subjected to pull-down assays. Lgl1-CΔ(645–677) was used as a negative control. NMII-A(1480–1842), but not NMII-A(1480–1816), bound to MBP-Lgl1-C, indicating that the interacting domain of Lgl1 to NMII-A is within residues 1817–1842 (Figure 3B). To test this hypothesis, we constructed an NMIIA Rod fragment (Figure 2B, NMII-AΔ(1812–1867) Rod) having an internal deletion of residues 1817–1842. The 28–amino acid charge periodicity that is necessary for NMII self-assembly (McLachlan and Karn, 1982; Atkinson and Stewart, 1992) was conserved. We found that this deletion abolished the binding of MBP-Lgl1-C to NMII-AΔ(1812–1867) Rod (Figure 3B). Together these results indicate that Lgl1 and NMII-A interact directly, and this interaction is mediated by residues 645–677 of Lgl1 and residues 1817–1842 of NMII-A Rod.

Lgl1 interferes with NMII-A filament assembly

Lgl1 binds to NMII-A via a region that is important for NMII filament assembly (Sohn *et al.*, 1997; Dulyaninova *et al.*, 2005;

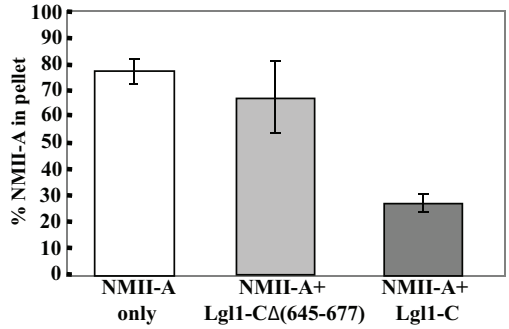

FIGURE 4: Lgl1 inhibits NMII-A filament assembly. NMII-A Rod alone or with Lgl1-C or Lgl1-CΔ(645–677) was subjected to filament assembly assay. Assays were performed using a buffer containing 10 mM phosphate buffer, pH 7.5, 2 mM $MgCl_2$, and 150 mM NaCl. Values represent the mean ± SD for three independent experiments.

Nakasawa *et al.*, 2005; Rosenberg *et al.*, 2008). Thus, Lgl1 binding to NMII-A Rod may affect its ability to assemble into filaments. To test this hypothesis, we assessed whether MBP-Lgl1-C binding to NMII-A had any effect on the assembly of NMII-A monomers into filaments. For this purpose we induced NMII-A Rod filament assembly in the presence of MBP-Lgl1-C or MBP-Lgl1-CΔ(645–677) as a negative control. At a molar ratio of two MBP-Lgl1-C per NMII-A Rod, only ~27% of the Rods assembled into filaments, compared with 78% of NMII-A Rods in filaments (Figure 4). Addition of Lgl1-CΔ(645–677), which is missing the NMII-A–binding domain, had only a minor effect on the assembly of NMII-A, with 67% of NMII-A Rods in filaments (Figure 4). These results indicate that Lgl1-C binding to NMII-A Rod shifts the monomer–polymer equilibrium of NMII-A toward the monomeric, unassembled state.

Lgl1 depletion affects NMII-A distribution in the cell leading edge and focal adhesion morphology

To discover whether Lgl1 regulates NMII-A filament assembly also in vivo, we characterized the cellular localization properties of these proteins in migrating cells. For this purpose we transfected fibroblast cells with construct encoding for GFP-Lgl1 and subjected them to wound scratch assay to achieve polarized migrating cells. In migrating polarized cells, GFP-Lgl1 colocalized with F-actin at the cell leading edge (Figure 5A and Supplemental Figure S1). NMII-A was present in the lamellum and absent from the lamellipodium (Figure 5A and Supplemental Figure S1) as previously described (Kolega, 1998; Gupton and Waterman-Storer, 2006; Vicente-Manzanares *et al.*, 2007). These observations were confirmed by quantification of the fluorescence intensity of GFP-Lgl1, F-actin, and NMII-A from the cell leading edge into the cell center (Figure 5B). NMII-A level was very low at the cell edge and rose gradually toward the cell center (Figure 5B). The fluorescence intensity of GFP-Lgl1 and F-actin revealed a similar pattern with maximum fluorescence at the cell edge (Figure 5B). These results confirm the presence of Lgl1 at the cell leading edge and its colocalization with F-actin and the absence of NMII-A from this region.

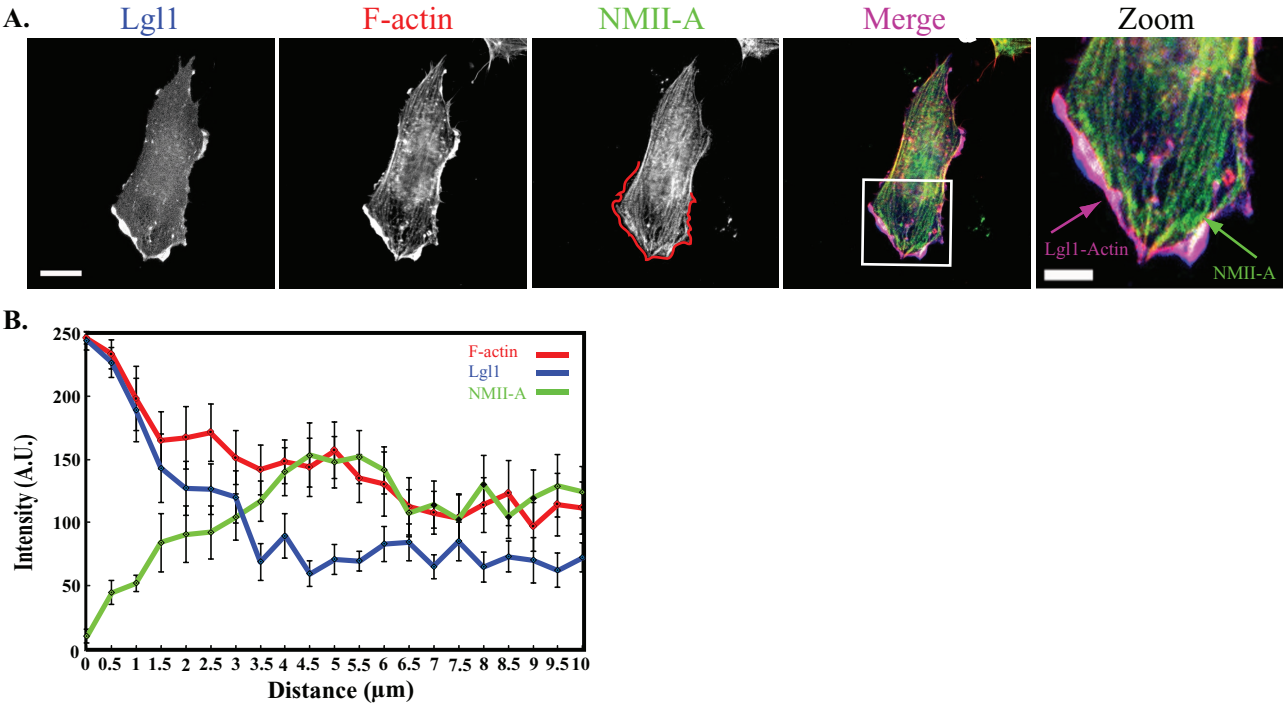

FIGURE 5: Lgl1 colocalizes with F-actin at the cell leading edge. (A) NIH 3T3 fibroblast cells were transfected with GFP-Lgl1, subjected to wound scratch assay, and stained for F-actin using rhodamine–phalloidin and for NMII-A using C-terminal–specific antibody conjugated to Cy5. The red line in the NMII-A column indicates the leading edge of the cell as determined by the F-actin staining. The white box in the merge column indicates the position of the inset for higher magnification shown in the rightmost column. Green and pink arrows in the rightmost column indicate the localization of NMII-A and the colocalization of Lgl-1 and F-actin, respectively. Bars in Lgl1 and Zoom, 20 and 10 μm, respectively. (B) Quantification of fluorescence intensity of Lgl1, F-actin, and NMII-A measured from the cell edge (0 μm) into the cell center (10 μm). The data shown are the mean ± SE of n ≥ 10 cells. The experiment was repeated at least three times with similar results. A.U., arbitrary units.

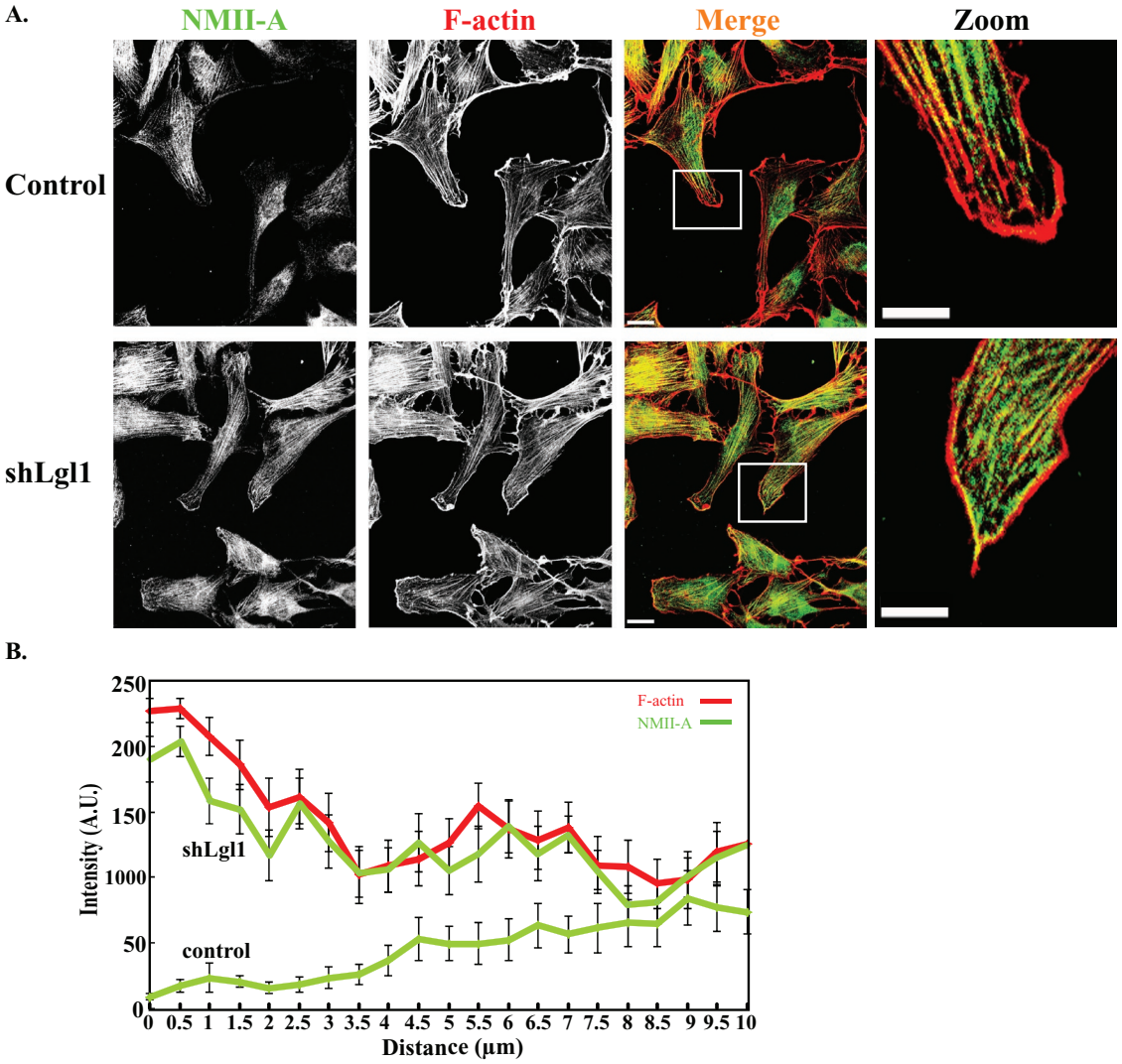

FIGURE 6: Lgl1 depletion displaces NMII-A to the cell leading edge. (A) shLgl1 and control cell lines were subjected to wound scratch assay and stained for NMII-A using C-terminal–specific antibody conjugated to Cy5. F-Actin was detected with rhodamine–phalloidin. White boxes in the Merge columns indicate the position of insets for higher magnification shown in the rightmost column. Bars in the Merge and Zoom columns, 20 and 10 μm, respectively. (B) Quantification of fluorescence intensity of NMII-A and F-actin for each indicated condition, measured from the cell edge (0 μm) into the cell center (10 μm). The values are the mean ± SE of n ≥ 16 cells for each condition. The experiment was repeated at least three times with similar results. A.U., arbitrary units.

To determine whether Lgl1 affects the spatial segregation of NMII-A during cell migration, we generated two knockdown vectors expressing small hairpin RNAs (shRNAs) specific for Lgl1, shLgl1-seq1, and shLgl1-seq2, respectively, that inhibit Lgl1 expression with high specificity. shLgl1-seq1 or shLgl1-seq2 treatment of NIH 3T3 fibroblasts leads to ~95% decrease in Lgl1 expression compared with control shRNA (Supplemental Figure S2). Furthermore, the expression of Lgl2 was not affected, indicating that the knockdown was specific for the Lgl1 isoform (Supplemental Figure S2). In the experiments described later we used shLgl1-seq1 and shLgl1-seq2 cell lines and referred to them as shLgl1 cells. To test whether Lgl1 affects the cellular localization of NMII-A in polarized migrating cells, shLgl1 cells were subjected to the wound scratch assay and stained for NMII-A and F-actin. Immunofluorescence localization of NMII-A indicated that whereas in control cells NMII-A was absent from lamellipodium, in shLgl1 cells NMII-A was localized in the lamellipodium along with F-actin (Figure 6A and Supplemental Figure S3). These observations were confirmed by quantification of the fluorescence intensity of NMII-A and F-actin from the leading edge into the cell center. In control cells the NMII-A level was very low in the first 4 μm adjacent to the cell edge (Figure 6B). In contrast, the fluorescence intensity of NMII-A in Lgl1-depleted cells indicated that it presented at the cell leading edge (Figure 6B). Furthermore, the fluorescence intensity pattern of NMII-A and F-actin in Lgl1-depleted cells was similar and the maximum fluorescence was detected at the cell edge (Figure 6B). These results confirm that in shLgl1 cells NMII-A presents at the cell leading edge and colocalizes with F-actin, indicating that in the absence of Lgl1, NMII-A reaches areas in the cell that normally are not accessible to this protein. Together with the findings that Lgl1 inhibits NMII-A filament assembly in vitro, these results may indicate that Lgl1 inhibits NMII-A filament assembly at the lamellipodium.

NMII-A mediates several major component processes that drive migration, among them the initiation and maturation of adhesion

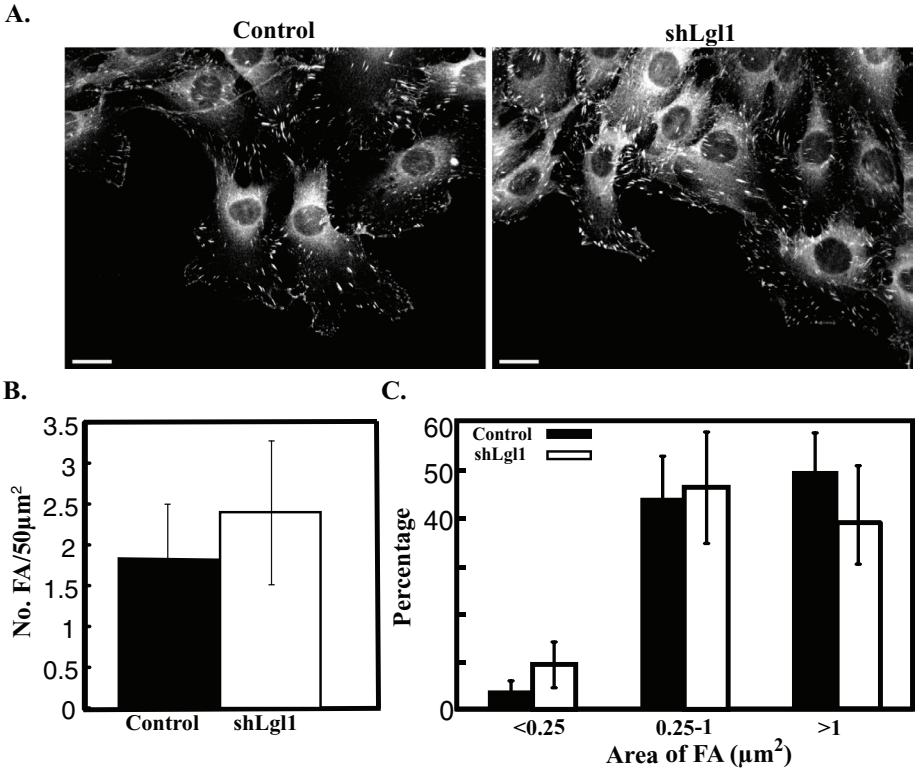

FIGURE 7: Lgl1 depletion affects the size and number of focal adhesions. (A) shLgl1 and control cells were subjected to wound scratch assay and immunostained with anti–mouse vinculin antibody. Bar, 20 μm. (B) Average number of focal adhesion sites per 50 μm^2 of cell protrusion. Values are the mean ± SD from three independent experiments subjected to two-tailed, two-sample, unequal-variance Student's *t* test, $p_{\text{control vs. shLgl1}} = 5.66e^{-5}$. (C) Size distribution of vinculin-containing focal adhesions (FAs; n ≥ 40 cells). Values are the mean ± SD from three independent experiments subjected to two-tailed, two-sample, unequal-variance Student's *t* test, $p_{\text{control vs. shLgl1 of FA<0.25 μm}^2} = 1.2e^{-7}$, $p_{\text{control vs. shLgl1 of FA= 0.25-1 μm}^2} = 0.32$, and $p_{\text{control vs. shLgl1 of FA>1 μm}^2} = 1.5e^{-4}$.

sites (Giannone *et al.*, 2007; Vicente-Manzanares *et al.*, 2007). Because the cellular localization of NMII-A in migrating cells is affected by Lgl1 depletion, we next assessed how the absence of Lgl1 could affect focal adhesion morphology in migrating polarized cells. Control cells showed well-defined adhesions in protrusions, as well as some small adhesions near the leading edge (Figure 7A) as described previously (Vicente-Manzanares *et al.*, 2007). In contrast, shLgl1 cells showed a marked increase in the number of focal adhesions (Figure 7B). To determine the role of Lgl1 in focal adhesion maturation, we analyzed the focal adhesion size in shLgl1 and control cells. Depletion of Lgl1 promoted small, nascent focal adhesions (<0.25 μm^2) and significantly decreased the proportion of large, mature focal adhesions (>1 μm^2) compared with control (Figure 7C). Collectively these results may suggest that Lgl1 is involved in the formation and maturation of focal adhesion via the regulation of NMII-A filament assembly.

Lgl1 depletion affects membrane dynamics and cell migration

NMII-A plays an important role in cell migration, as it is essential for the retraction of the cell edges, as well as for adhesion maturation at the cell front (Vicente-Manzanares *et al.*, 2007). To determine whether the abnormal cellular localization of NMII-A and focal adhesion morphology upon Lgl1 depletion are accompanied by alterations in cell spreading, membrane dynamics during spreading of control and shLgl1 cells was examined by time-lapse video microscopy. On adhesion, control cells generally produced stable lamellipodia that gradually extended and did not collapse or retract back into the cell body. By contrast, shLgl1 cells extended and retracted numerous short-lived protrusions, resulting in a highly irregular peripheral edge (Figure 8 and Supplemental Movies S1 and S2). These data show that Lgl1 depletion leads to high levels of activity at the cell periphery that are characterized by the rapid formation and retraction of small protrusions. Together these results indicate that Lgl1 affects membrane dynamics by the regulation of focal adhesion formation.

To determine whether Lgl1 affects cell migration, we assessed the ability of shLgl1 cells to initiate migration in a wound scratch assay. In contrast to control cells that migrated in one sheet to close the wound, some of the shLgl1 cells detached from the cell sheet and moved in different directions as single cells or as a group of few cells (Figure 9A). Furthermore, Lgl1-depleted cells had elongated morphology with long extensions (Figure 9A, arrows), whereas control cells exhibited broad lamellipodia (Figure 9A, arrowheads). To further examine the behavior of shLgl1 cells, cells that had been subjected to the wound scratch assay were stained for F-actin (Figure 9B). It is apparent that control cells formed one sheet with the same cell polarity as determined by the orientation of F-actin. In contrast, shLgl1 cells exhibited different cell polarities, with some cells detached from the main sheet. Collectively these results indicate that depletion of Lgl1 resulted in a loss of cell–cell contact and in independent migration of detached cells into the wound space. The aberrant migration of Lgl1-depleted cells meant that it was difficult to determine the rate of wound closure by shLgl1 cells. We therefore quantified the wound-induced migration during the first 2 h of wound healing. The migration rate of shLgl1 was more than twofold higher than that of control cells (33.5 ± 4.71 and 15 ± 4.65 μm/h, respectively; Figure 9C). These results are consistent with the findings that reexpression of Lgl1 in melanoma cell lines that have low levels of Lgl1 expression decreases cell migration and increases cell adhesion (Kuphal *et al.*, 2006). Collectively these results indicate that depletion of Lgl1 leads to aberrant cell migration.

DISCUSSION

Lgl1, an evolutionarily conserved and widely expressed cytoskeletal protein, is indispensable for the establishment and maintenance of cell polarity (for review see Assemat *et al.*, 2008). However, the mechanism by which Lgl1 contributes to the establishment of migrating cell polarity is poorly understood. Our data provide a step toward understanding this mechanism. We showed that Lgl1 interacts directly with NMII-A and inhibits NMII-A filament assembly. Furthermore, in the absence of Lgl1, NMII-A localizes to the cell leading edge, a region that is normally uninhabited by NMII-A, and focal adhesion appeared prematurely, leading to abnormal membrane dynamics and cell migration.

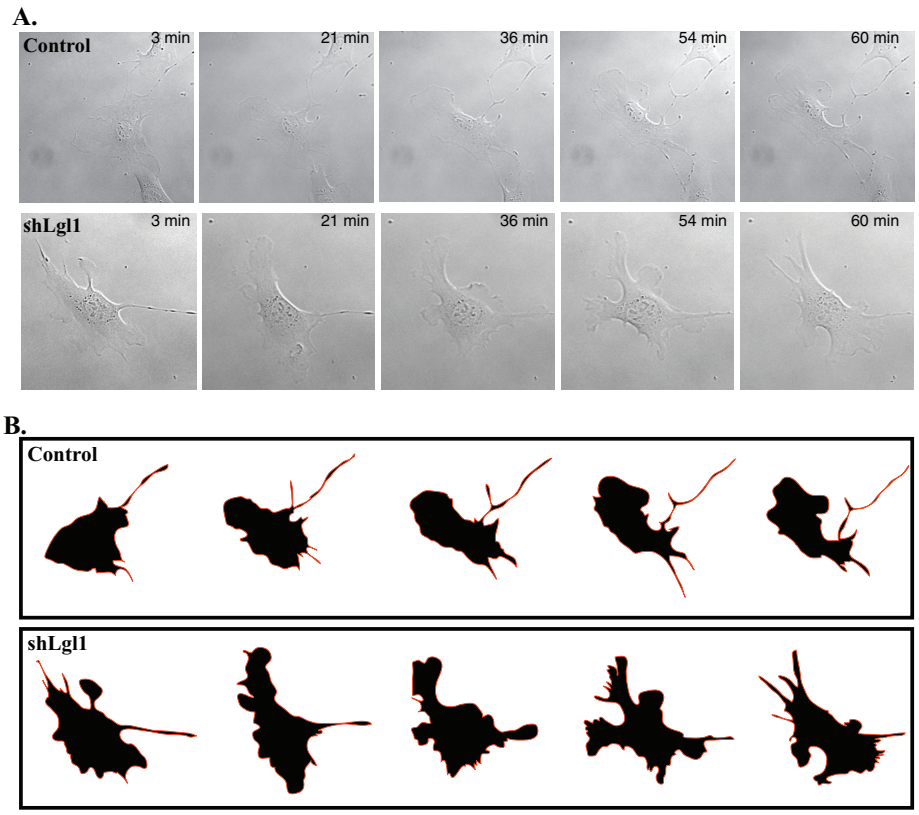

FIGURE 8: The effect of Lgl1 on membrane dynamics. (A) Membrane dynamics of shLgl1 and control cell lines was analyzed using time-lapse confocal microscopy. Representative images at the indicated time points of the movie are shown. (B) Contours of the cell boundaries of the selected shLgl1 and control cells displayed in A.

Using the pull-down assay, we identified residues 1816–1842 of the NMII-A heavy chain as the Lgl1-interacting domain. This site maps to a region that is important for NMII filament assembly (Sohn *et al.*, 1997; Dulyaninova *et al.*, 2005; Nakasawa *et al.*, 2005; Rosenberg *et al.*, 2008). Sohn *et al.* (1997) identified a 29–amino acid region near the C-terminal end that is essential for filament formation and named it the assembly-competent domain (ACD). Further analysis of this region indicated that within the 29 amino acids of the ACD there are four positively charged amino acids (1918, 1920, 1922, and 1923) that are crucial for filament assembly (Figure 10A; Straussman, 2005). Previous work in our laboratory identified four negatively charged amino acids (1820, 1821, 1824, and 1826) starting 98 amino acids N-terminal to the ACD (Figure 10A) that are also important for filament assembly (Straussman, 2005), and this region was termed the complementary ACD (cACD). The 98–amino acid distance between the ACD and the cACD equals the stagger between every two myosin II molecules that build an antiparallel filament (Huxley, 1957). We proposed that in the process of NMII filament assembly, the ACD region of a new NMII Rod that joins a growing filament interacts with the cACD region of another NMII molecule. The distance between the ACD and the cACD must therefore equal the stagger. Attraction between the ACD and cACD regions can thus direct the joining rod and dictate the stagger (Straussman, 2005).

Examination of the Lgl1 and NMII-A interacting domains indicated that the Lgl1 domain, which contains positive amino acids, binds to a region of NMII-A that contains the negatively charged cACD (Figure 10B). It is therefore plausible that Lgl1 inhibits NMII-A filament assembly by binding to the cACD and preventing it from interaction with the ACD— a process that is required for filament assembly. The Lgl1 domain that interacts with NMII-A is positively charged and contains the phosphorylation sites for aPKCζ (Figure 10B). We propose that the interaction between Lgl1 and NMII-A is electrostatic, and phosphorylation of Lgl1 by aPKCζ decreases the positive charge of the Lgl1-interacting domain, thus preventing the binding of Lgl1 to NMII-A and so regulating the interaction between Lgl1 and NMII-A. Support for this hypothesis comes from the findings that phosphorylation of *Drosophila* Lgl dissociates it from the cytoskeleton (Betschinger *et al.*, 2005).

Cell migration is a highly regulated and coordinated process. It comprises several different yet integrated steps, which include polarization, protrusion, and adhesion formation and turnover at the cell front, along with adhesion disassembly and tail retraction at the cell rear (for review see Lauffenburger and Horwitz, 1996; Ridley *et al.*, 2003). In migrating fibroblasts, the NMII isoforms play different roles in cell polarization. NMII-A is dynamic and assembles actomyosin bundles in protrusions; by contrast, NMII-B incorporates into preformed F-actin bundles and remains stationary, defining the center and rear of the migrating cell (for review see Vicente-Manzanares *et al.*, 2008). Our observations provide new insights into the mechanism by which NMII-A is excluded from lamellipodial extensions of migrating fibroblasts. We showed that Lgl1 presents in the cell leading edge, facilitating NMII-A exclusion from this region. In the absence of Lgl1, NMII-A is able to reach cellular regions that are not accessible to it when Lgl1 presents. Our results are consistent with the findings that asymmetric segregation in *Drosophila* neuroblasts is achieved in part by the restriction of NMII to the apical cortex by Lgl (Barros *et al.*, 2003).

An important step in cell migration is the formation and turnover of adhesion at the cell front. Although the formation of nascent focal complexes is NMII-A independent, the formation of fully developed, mature focal adhesion requires NMII-A motor activity (Choi *et al.*, 2008). Mature adhesions are believed to transmit strong forces from the cytoskeleton to the extracellular matrix (Vicente-Manzanares *et al.*, 2009a) to promote adhesion turnover in cell migration (Webb *et al.*, 2004; Zaidel-Bar *et al.*, 2007). We suggest that the decrease in focal adhesion maturation in shLgl1 cells is the result of the unusual cellular localization of NMII-A in the cell leading edge. Finally, we provided a clue for the role of Lgl1 in establishing cell polarity of migrating cells. We demonstrated that Lgl1-knockdown cells present two unique characterizations during migration—detachment from the cell sheet and migration in different directions, in contrast to control cells, which move as one sheet in one direction. We propose that cell polarity of migrating cells is achieved by excluding NMII-A from the cell leading edge by Lgl1. The failure to exclude NMII-A from the leading edge of cells results in the appearance of nonpolarized cells and their detachment from the cell sheet. We further suggest that the faster migration of Lgl1-depleted cells compared with control cells is caused by movement of these cells in groups or as single cells and not as one sheet. It is therefore

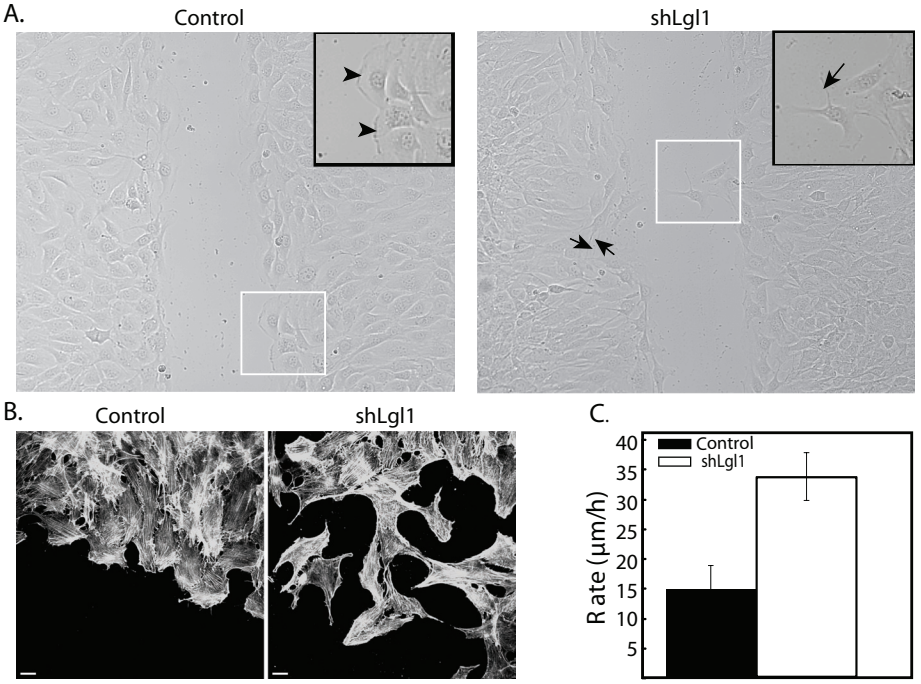

FIGURE 9: The effect of Lgl1 on directed cell migration. (A) Migration of shLgl1 and control cell lines was stimulated by scratching a cell monolayer with a pipette tip and analyzed by time-lapse confocal microscopy. Shown are images taken 5 h after the scratch. White boxes indicate the position of insets for higher magnification shown in the left corner for each cell line image. Arrowheads point to the broad lamellipodia exhibited by control cells. Arrows point to cell extensions exhibited by Lgl1-depleted cells. (B) shLgl1 and control cells were subjected to wound scratch, fixed, and stained for F-actin with rhodamine–phalloidin. Bar, 20 µm. (C) The average rate of wound closure 2 h after wounding. Values are the mean ± SD from three independent experiments subjected to two-tailed, two-sample, unequal-variance Student's *t* test, $p_{control\ vs.\ shLgl1} = 1.4\ e^{-3}$.

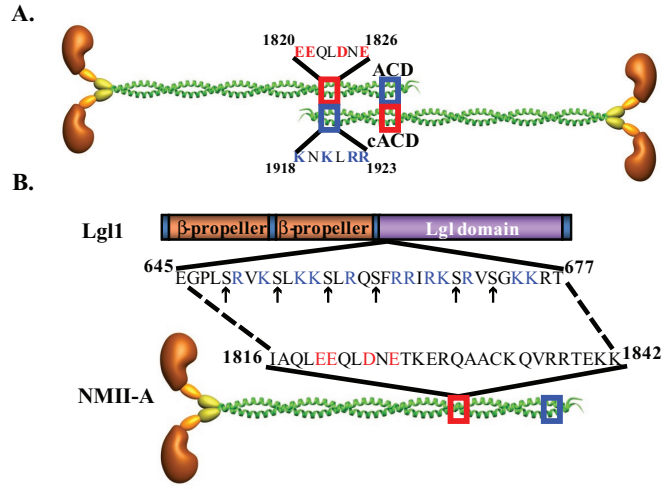

FIGURE 10: A model depicting the role of Lgl1 binding to NMII-A. (A) Schematic presentation of the role of ACD and cACD in NMII-A filament assembly. The sequences important for the interaction between NMII-A monomers are indicated. (B) Lgl1 and NMII-A interacting domain sequences. Arrows indicate the serines that are phosphorylated by aPKCζ. Positively charged amino acids are indicated in blue, and negatively charged amino acids are indicated in red. ACD, blue frame; cACD, red frame. Numbers represent amino acid positions in the full-length proteins.

possible that cells in sheets move more slowly because of cell–cell contact.

MATERIALS AND METHODS

The proteins used for this study were NMII-A, Lgl1, and Lgl2, with accession numbers NP_002473, NM_008502, and NM_145438, respectively.

Cell lines and culture conditions

Mouse embryonic fibroblast NIH 3T3, Cos-7, human colon cancer SW620, and HEK293T cell lines were maintained in high-glucose DMEM supplemented with 2 mM L-glutamine, 10% fetal calf serum, and antibiotics (100 U/ml penicillin, 100 mg/ml streptomycin, and 1:100 Biomyc3 anti-mycoplasma antibiotic solution; Biological Industries, Beit HaEmek, Israel). Cells were grown at 37°C in a humidified atmosphere of 5% CO_2 and 95% air.

Antibodies

Antibodies specific to the C-terminal region of mouse NMII-A and platelet NMII antibodies were gift from R. S. Adelstein (National Institutes of Health). Antibodies specific to the C-terminal region of human NMII-A were generated in rabbits as described (Phillips *et al.*, 1995). Recombinant GFP antibodies were prepared in rabbits as described (Rosenberg and Ravid, 2006). Specific antibodies against the C- and N-terminal domains of Lgl1 and N-terminal of Lgl2 were generated in rabbit using the peptides DTTLDTTGDVTVEDVKD, DDYRCGKALGPVESLQ, and GHDPARERLKRDLFQ, respectively. Vinculin and β-actin mouse monoclonal antibodies were purchased from Sigma-Aldrich (St. Louis, MO).

Construction of Lgl1 mutants

Lgl1 and pMBP-3 (Sheffield *et al.*, 1999) were kindly provided by T. Pawson (University of Toronto) and P. Sheffield (University of Virginia), respectively. To create pMBP-Lgl1, Lgl1 in pCMV5 vector was digested with *Bam*HI, and the fragment was inserted into pMBP-3 that was digested with *Bam*HI. To create pMBP-Lgl1-N, pMBP-Lgl1 was digested with *Eco*RI and *Bsp*68I, followed by fill-in reaction using Klenow fragment and self-ligation. To create pMBP-Lgl1-C, pMBP-Lgl1 was digested with *Eco*RI and *Bsp*68I, and the fragment was inserted into pMBP-2 that was digested with *Eco*RI–*Sma*I. To create pMBP-Lgl1(678–1036), an *Eco*RI site was added to pMBP-Lgl1-C using a QuikChange Site-Directed Mutagenesis Kit (Stratagene, La Jolla, CA) according to the manufacturer's instructions, using the primer 5′-GCC GTG TCT CAG GCA AAA AAC GAA TTC CTG CTG CCA GTA G-3′, followed by digestion with *Eco*RI. This fragment was cloned into pMBP-2 that was digested with *Eco*RI. To create pMBP-Lgl1(740–1036), pMBP-Lgl1-C was digested with *Apa*I and fill-in reaction using Klenow fragment, followed by *Eco*RI digestion. The restricted fragment was inserted into pMBP-1 that was digested with *Bam*HI and fill-in reaction using Klenow fragment, followed by *Eco*RI digestion. To create pMBP-Lgl1(615–1036), pMBP-Lgl1 was digested with *Kpn*I, and the fragment was inserted into pMBP-2 that was digested with *Kpn*I.

To create pMBP-Lgl1-CΔ(645-677), *Mun*I site was added to pMBP-Lgl1-C by site-directed mutagenesis using primer 5′-CCC CAA TGAT TCT TTG GCA ATT GAG GGG CCA CTG TC-3′, followed by digestion with *Eco*RI and *Mun*I to get three fragments, 96 base pairs,1.3 kb, and 7 kb, and the last two fragments were ligated. To achieve the correct reading frame, the vector was subjected to site-directed mutagenesis with the primer 5′-CAA TGA TTC TTT GGC AAC TCC TGC TGC CAG TAG C-3′. To create pGFP-Lgl1, pMBP-Lgl1 was digested with *Bam*HI, and the fragment was ligated into pGFP-C2 plasmid digested with *Bam*HI.

Construction of NMII-A Rod mutants

pGFP-NMII-A was a kind gift from R. S Adelstein. To create pET21-NMII-A(1480–1816), a terminator codon was added to pET21-NMII-A-Rod (Ronen and Ravid, 2009) by site-directed mutagenesis using primer 5′-CCT CGA GGC CAA GAT TTG ACA GCT GGA GGA GC-3′. To create pET21-NMII-A(1480–1842), a terminator codon was added in pET21-NMII-A-Rod by site-directed mutagenesis using primer 5′- GTC GGA CCG AGA AGT AGC TGA AGG ATG TGC-3′. To create pET21-NMII-AΔ(1812–1867), two *Aat*II sites were added in pET21-NMII-A-Rod by site-directed mutagenesis using the primers 5′-GGC CTC CAT CAC CGA CGT CGA GGC CAA-3′ and 5′-CCA GGC CGA CAA GAC GTC TAC CCG CCT GAA G-3′. The plasmid was digested with *Aat*II and self-ligated. To achieve the correct reading frame, the plasmid was subjected to site-directed mutagenesis with the primer 5′-CCT CCA TCA CCG CAG CGT CTA CCC GCC-3′. To create Cherry-NMII-A, pmCherry-C3 (provided by Michael Brandeis, Hebrew University of Jerusalem, Jerusalem, Israel) was digested with *Nde*I and *Sca*I, and the fragment was cloned into pGFP-NMII-A digested with *Nde*I and *Sca*I.

Bacterial expression and purification of MBP-Lgl1 and NMII-A protein fragments

pMBP-Lgl1 constructs were transformed to *Escherichia coli* BL21-CodonPlus(DE3)-RIL (obtained from Tsafi Danieli, Hebrew University of Jerusalem), and the bacteria were grown in 100 ml of Luria broth (LB) with 50 µg/ml ampicillin at 37°C to $OD_{600\ nm} = 0.5$, and then 0.1 mM isopropyl-β-D-thiogalactoside was added and the bacteria were grown for an additional 3 h at 25°C. The bacteria were pelleted at 12,000 × *g* at 4°C for 20 min, and the pellets were frozen at –20°C. The bacterial pellet was dissolved in 4 ml of MBP buffer (20 mM Tris-HCl, pH 7.5, 5 mM $MgCl_2$, 150 mM NaCl, 1 mM dithiothreitol [DTT], and 0.1 mM phenylmethylsulfonyl fluoride [PMSF]) and 1 mg/ml lysozyme and incubated on ice for 15 min. The lysate was sonicated for 5 × 10 s (Misonix Microson Ultrasonic Cell Disruptor, Qsonica, Newtown, CT) and centrifuged at 16,000 × *g* at 4°C for 20 min. Five hundred microliters of 50% amylose beads slurry (New England BioLabs, Ipswich, MA) were washed twice with MBP buffer, added to the bacterial lysate, and incubated at 4°C for 2 h on rotator, followed by three washes with MBP buffer. Expression and purification of NMII-A Rod fragments were carried out as described (Straussman *et al.*, 2007). The concentrations of the MBP-Lgl1 proteins bound to amylase beads and of NMII-A Rod fragments were determined by comparing the densitometry of the band of a sample of each protein on Coomassie-stained PAGE to known amounts of bovine serum albumin samples on the same gel.

Binding of MBP-Lgl1 fusion proteins to cell extract proteins

SW620 cells were grown on 60-mm plates to 60–80% confluence and lysed with ice-cold CHAPS buffer (50 mM Tris-HCl, pH 7.5, 150 mM NaCl, 5 mM EDTA, 5 mM ethylene glycol tetraacetic acid, 1% 3-[(3-cholamidopropyl)dimethylammonio]-1-propanesulfonate, 1 mM DTT, and protease inhibitors cocktail [Sigma-Aldrich]), incubated on ice for 15 min, and centrifuged at 16,000 × *g* at 4°C for 15 min. The supernatants were incubated at 4°C for 2 h with MBP-Lgl1 or MBP-Lgl1-C bound to amylase beads, followed by three washes with CHAPS buffer. Samples were separated on 7% SDS–PAGE, and Western blotting was performed using anti-human NMII-A and Lgl1 antibodies.

Coimmunoprecipitation and Western blotting

pGFP or pGFP-Lgl1 and mCherry-NMII-A were cotransfected to ~70% confluent Cos-7 or HEK293T cell lines in 30- or 100-mm plates using polyethylenimine (Sigma-Aldrich) transfection reagent. At 48 h after transfection the cells were washed three times with ice-cold phosphate-buffered saline (PBS) and lysed with 1 ml NP-40 buffer (10 mM Tris-HCl, pH 8, 1 mM EDTA, 100 mM NaCl, 1 mM DTT, and 0.5% NP-40) containing protease inhibitor cocktail (Sigma-Aldrich). Cells were then sonicated, incubated for 15 min on ice, and centrifuged at 25,000 × *g* at 4°C for 15 min. A 50-µl amount of the supernatants was used for input control, and the rest of the supernatants was transferred to fresh tubes containing protein A agarose beads (Pierce, Rockford, IL) coupled to GFP or NMII-A antibodies and rotated at 4°C for 2 h, followed by four washes with NP-40 buffer. Samples were dissolved in SDS–PAGE sample buffer, separated on 7% SDS–PAGE, and subjected to Western blotting using anti–human NMII-A and anti-GFP antibodies.

Pull-down assay

A total of 15 µg of MBP-Lgl1 protein fragments immobilized on amylose beads in 500 µl of CHAPS buffer was incubated with 6 µg of NMII-A Rod fragments at 4°C for 2 h using a rotator. Bound proteins were washed three times in CHAPS buffer, resolved by 10% SDS–PAGE, and analyzed by Western blots with anti-Lgl1, anti–NMII-A, or anti–platelet NMII.

Inhibition of NMII-A filament assembly by Lgl1-C

Maltose 0.1 M was added to 1.2 ml of MBP-Lgl1-C or MBP-Lgl1-CΔ(645–677) immobilized on amylose beads, incubated on rotator for 1 h at 4°C, and centrifuged at 6000 × *g* at 4°C for 2 min. The supernatants were dialyzed against MBP buffer containing 1 mM DTT and 0.1 mM PMSF. Proteins concentration was determined as described. MBP-Lgl1-C or MBP-Lgl1-CΔ(645–677) at 3–6 µM was added to monomeric NMII-A Rod in 20 mM Tris-HCl (pH 7.5), 600 mM NaCl, 5 mM EDTA, and 1 mM DTT and dialyzed against 10 mM phosphate buffer, pH 7.5, 2 mM $MgCl_2$, and 150 mM NaCl for 4 h at 4°C. The protein mix was centrifuged in a TL-100 ultracentrifuge (Beckman Coulter, Fullerton, CA) at 100,000 × *g*, at 4°C for 1 h, and the supernatant and pellet were separated on 10% SDS–PAGE. The gels were stained with Coomassie brilliant blue, scanned, and quantified using the densitometry program ImageGauge V (Fujifilm, Tokyo, Japan).

Creating shRNA-depleted cell lines

Lgl1 shRNA sequence 5′-CGC GTC CCC ACC AAA TCC TCA TTG GCT ATT CAA GAG ATA GCC AAT GAG GAT TTG GTT TTT TGG AAA T-3′ (shLgl1-seq1) or 5′-CGC GTC CCC GCT TAC GTC TGC TCT ACA AAC TTC AAG AGA GTT TGT AGA GCA GAC GTA AGC TTT TTG GAA AT-3′ (ShLgl1-seq2) were inserted into pLVHTM (LentiWeb, http://lentiweb.com), according to the manufacturer's instructions. This plasmid has an independent GFP protein transcribed as an infection marker. Control sequence 5′-CGC GTC CCC GAG CAC TTA AGG AAT GAG TTT CAA GAG AAC TCA TTC CTT AAG TGC TCT TTT TGG AAA T-3′ was created in a similar manner.

shRNA plasmids were transfected into HEK293T cells, and 48 h after transfection, lentivirus-containing medium was collected, filtered through a 0.45-μm filter, and centrifuged for 2 h at 45,000 × *g* to collect the lentivirus particles. The particles were resuspended in 500 μl of serum-free medium containing polybrene (Sigma-Aldrich) and incubated on ice for 30 min. NIH 3T3 cells were infected with the lentivirus particles for 4 h with constant rocking. To determine the expression levels of Lgl1 and Lgl2, shLgl1-seq1 and shLgl1-seq2 and control cell lines were subjected to Western blot analysis with antibodies specific for Lgl1 and Lgl2.

Wound scratch assay and confocal microscopy

A total of 2×10^5 NIH 3T3 cells was seeded on coverslips coated with 10 μg/ml fibronectin and transfected with pGFP-Lgl1 using polyethylenimine transfection reagent (Sigma-Aldrich). At 48 h posttransfection the cells were washed twice with 1 ml of starvation medium (high-glucose DMEM supplemented with 2 mM L-glutamine, 100 U/ml penicillin, 100 μg/ml streptomycin, 12 mM 4-(2-hydroxyethyl)-1-piperazineethanesulfonic acid, pH 7.4, and 0.1% fatty acid–free bovine serum albumin [Sigma-Aldrich]) and serum starved for 3 h. Three parallel scratches were performed using a small pipette tip, and the cells were washed twice with starvation medium to remove cell debris. Then high-glucose DMEM medium was added, and cells were incubated for 7 h. Cells were washed three times with PBS and fixed for 30 min in 1.5 ml of 3.7% formaldehyde in PBS. shLgl1 and shRNA control cells were treated as described except that they were serum starved for 16 h before performing the scratches and incubated for 3 h in high-glucose DMEM medium before fixation. The three cell lines were immunostained with anti-mouse NMII-A antibody and secondary antibody conjugated to Cy5. F-Actin was stained with rhodamine–phalloidin as described (Ronen and Ravid, 2009). For focal adhesions analysis, shLgl1 and shRNA control cells were immunostained with vinculin antibody. Cells were visualized using a 60× magnification, numerical aperture 1.4 objective under a TE2000 inverted confocal laser scanning system (Nikon, Tokyo, Japan). Consecutive Z-stakes were taken using a small aperture and converged to create one image using EZ-C1 software (Nikon). Quantification of the fluorescence of GFP-Lgl1, F-actin, and NMII-A as a function of the distance from the cell edge was performed using the ImageJ software package (National Institutes of Health, Bethesda, MD). Focal adhesion area and number measurements were also performed using the ImageJ software package and the results subjected to a two-tailed, two-sampled, unequal-variance Student's *t* test using at least 60 cells.

To determine the rate of wound closure, shLgl1 and shRNA control cells were subjected to wound scratch assay as described. Phase-contrast images of the wound area were taken just after the wounding, and the wound area was imaged at different times over a 24-h period. Wound widths were measured at a minimum of four different points of each wound, and the average rate of wound closure during the first 2 h of wound healing was calculated.

Live-cell imaging

shLgl1 and control cell lines were seeded on a Lab-Tek (Nalge Nunc International, Rochester, NY) two-well chamber coated with10 μg/ml fibronectin and were visualized using time-lapse confocal microscopy every 3 min for 1.5 h using a 40× objective. Images were processed and converted to QuickTime (Apple, Cupertino, CA) movies using ZEN2009 and ImageJ software.

ACKNOWLEDGMENTS

We thank Robert S. Adelstein for the NMII-A construct and NMII-A antibodies, Peter Sheffield for MBP constructs, and Tzafi Danieli for Codon-Plus bacteria. We are grateful to Daniel Ronen and Michael Rosenberg for discussions throughout the course of these studies and for invaluable comments on the manuscript. We thank Michael Rosenberg and Dvir Aran for help with the statistics and Lea Baraz for carefully reading the manuscript. This research project was support in part by a grant from the Israel Cancer Association and one from the U.S. Agency for International Development American Schools and Hospitals Abroad Program for the procurement of the confocal LSM710 microscope.

REFERENCES

Assemat E, Bazellieres E, Pallesi-Pocachard E, Le Bivic A, Massey-Harroche D (2008). Polarity complex proteins. Biochim Biophys Acta 1778, 614–630.

Atkinson SJ, Stewart M (1992). Molecular interactions in myosin assembly. Role of the 28-residue charge repeat in the rod. J Mol Biol 226, 7–13.

Barros CS, Phelps CB, Brand AH (2003). *Drosophila* nonmuscle myosin II promotes the asymmetric segregation of cell fate determinants by cortical exclusion rather than active transport. Dev Cell 5, 829–840.

Betschinger J, Eisenhaber F, Knoblich JA (2005). Phosphorylation-induced autoinhibition regulates the cytoskeletal protein Lethal (2) giant larvae. Curr Biol 15, 276–282.

Bilder D, Li M, Perrimon N (2000). Cooperative regulation of cell polarity and growth by *Drosophila* tumor suppressors. Science 289, 113–116.

Bilder D, Perrimon N (2000). Localization of apical epithelial determinants by the basolateral PDZ protein Scribble. Nature 403, 676–680.

Bresnick AR (1999). Molecular mechanisms of nonmuscle myosin-II regulation. Curr Opin Cell Biol 11, 26–33.

Choi CK, Vicente-Manzanares M, Zareno J, Whitmore LA, Mogilner A, Horwitz AR (2008). Actin and alpha-actinin orchestrate the assembly and maturation of nascent adhesions in a myosin II motor-independent manner. Nat Cell Biol 10, 1039–1050.

Conti MA, Adelstein RS (2008). Nonmuscle myosin II moves in new directions. J Cell Sci 121, 11–18.

Dulyaninova NG, Malashkevich VN, Almo SC, Bresnick AR (2005). Regulation of myosin-IIA assembly and Mts1 binding by heavy chain phosphorylation. Biochemistry 44, 6867–6876.

Etienne-Manneville S (2008). Polarity proteins in migration and invasion. Oncogene 27, 6970–6980.

Even-Faitelson L, Ravid S (2006). PAK1 and aPKCζ regulate myosin II-B phosphorylation: a novel signaling pathway regulating filament assembly. Mol Biol Cell 17, 2869–2881.

Giannone G *et al*. (2007). Lamellipodial actin mechanically links myosin activity with adhesion-site formation. Cell 128, 561–575.

Golomb E, Ma X, Jana SS, Preston YA, Kawamoto S, Shoham NG, Goldin E, Conti MA, Sellers JR, Adelstein RS (2004). Identification and characterization of nonmuscle myosin II-C, a new member of the myosin II family. J Biol Chem 279, 2800–2808.

Gupton SL, Waterman-Storer CM (2006). Spatiotemporal feedback between actomyosin and focal-adhesion systems optimizes rapid cell migration. Cell 125, 1361–1374.

Huxley AF (1957). Muscle structure and theories of contraction. Prog Biophys Biophys Chem 7, 225–318.

Kalmes A, Merdes G, Neumann B, Strand D, Mechler BM (1996). A serine-kinase associated with the p127-l(2)gl tumour suppressor of *Drosophila* may regulate the binding of p127 to nonmuscle myosin II heavy chain and the attachment p127 to the plasma membrane. J Cell Sci 109, 1359–1368.

Klezovitch O, Fernandez TE, Tapscott SJ, Vasioukhin V (2004). Loss of cell polarity causes severe brain dysplasia in Lgl1 knockout mice. Genes Dev 18, 559–571.

Kolega J (1998). Cytoplasmic dynamics of myosin IIA and IIB: spatial "sorting" of isoforms in locomoting cells. J Cell Sci 111, 2085–2095.

Kuphal S, Wallner S, Schimanski CC, Bataille F, Hofer P, Strand S, Strand D, Bosserhoff AK (2006). Expression of Hugl-1 is strongly reduced in malignant melanoma. Oncogene 25, 103–110.

Lauffenburger DA, Horwitz AF (1996). Cell migration: a physically integrated molecular process. Cell 84, 359–369.

McLachlan AD, Karn J (1982). Periodic charge distributions in the myosin rod amino acid sequence match cross-bridge spacings in muscle. Nature 299, 226–231.

Murakami N, Kotula L, Hwang Y-W (2000). Two distinct mechanisms for regulation of nonmuscle myosin assembly via the heavy chain: phosphorylation for MIIB and Mts 1 binding for MIIA. Biochemistry 39, 11441–11451.

Nakasawa T, Takahashi M, Matsuzawa F, Aikawa S, Togashi Y, Saitoh T, Yamagishi A, Yazawa M (2005). Critical regions for assembly of vertebrate nonmuscle myosin II. Biochemistry 44, 174–183.
Ohshiro T, Yagami T, Zhang C, Matsuzaki F (2000). Role of cortical tumour-suppressor proteins in asymmetric division of *Drosophila* neuroblast. Nature 408, 593–596.
Peng CY, Manning L, Albertson R, Doe CQ (2000). The tumour-suppressor genes lgl and dlg regulate basal protein targeting in *Drosophila* neuroblasts. Nature 408, 596–600.
Phillips CL, Yamakawa K, Adelstein RS (1995). Cloning of the cDNA encoding human nonmuscle myosin heavy chain-B and analysis of human tissues with isoform-specific antibodies. J Muscle Res Cell Motil 16, 379–389.
Plant PJ, Fawcett JP, Lin DC, Holdorf AD, Binns K, Kulkarni S, Pawson T (2003). A polarity complex of mPar-6 and atypical PKC binds, phosphorylates and regulates mammalian Lgl. Nat Cell Biol 5, 301–308.
Ridley AJ, Schwartz MA, Burridge K, Firtel RA, Ginsberg MH, Borisy G, Parsons JT, Horwitz AR (2003). Cell migration: integrating signals from front to back. Science 302, 1704–1709.
Ronen D, Ravid S (2009). Myosin II tailpiece determines its paracrystal structure, filament assembly properties, and cellular localization. J Biol Chem 284, 24948–24957.
Rosenberg M, Ravid S (2006). Protein kinase Cγ regulates myosin IIB phosphorylation, cellular localization, and filament assembly. Mol Biol Cell 17, 1364–1374.
Rosenberg M, Straussman R, Ben-Ya'acov A, Ronen D, Ravid S (2008). MHC-IIB filament assembly and cellular localization are governed by the rod net charge. PLoS ONE 3, e1496.
Schimanski CC *et al.* (2005). Reduced expression of Hugl-1, the human homologue of *Drosophila* tumour suppressor gene lgl, contributes to progression of colorectal cancer. Oncogene 24, 3100–3109.
Sheffield P, Garrard S, Derewenda Z (1999). Overcoming expression and purification problems of RhoGDI using a family of "parallel" expression vectors. Protein Expr Purif 15, 34–39.
Shohet RV, Conti MA, Kawamoto S, Preston YA, Brill DA, Adelstein RS (1989). Cloning of the cDNA encoding the myosin heavy chain of a vertebrate cellular myosin. Proc Natl Acad Sci USA 86, 7726–7730.
Simons M, Wang M, McBride OW, Kawamoto S, Yamakawa K, Gdula D, Adelstein RS, Weir L (1991). Human nonmuscle myosin heavy chains are encoded by two genes located on different chromosomes. Circ Res 69, 530–539.
Sohn RL, Vikstrom KL, Strauss M, Cohen C, Szent-Gyorgyi AG, Leinwand LA (1997). A 29 residue region of the sarcomeric myosin rod is necessary for filament formation. J Mol Biol 266, 317–330.
Sripathy S, Lee M, Vasioukhin V (2011). Mammalian Llgl2 is necessary for proper branching morphogenesis during placental development. Mol Cell Biol 31, 2920–2933.
Strand D, Jakobs R, Merdes G, Neumann B, Kalmes A, Heid HW, Husmmann I, Mechler M (1994a). The *Drosophila* lethal(2)giant larvae tumor suppressor protein forms homo-oligomers and is associated with nonmuscle myosin II heavy chain. J Cell Biol 127, 1361–1373.
Strand D, Raska I, Mechler BM (1994b). The *Drosophila* lethal(2)giant larvae tumor suppressor protein is a component of the cytoskeleton. J Cell Biol 127, 1345–1360.
Straussman R (2005). New insights into the assembly properties of myosin II. PhD thesis, Hebrew University of Jerusalem, Jerusalem, Israel.
Straussman R, Ben-Ya'acov A, Woolfson DN, Ravid S (2007). Kinking the coiled coil-negatively charged residues at the coiled-coil interface. J Mol Biol 366, 1232–1242.
Tan JL, Ravid S, Spudich JA (1992). Control of nonmuscle myosins by phosphorylation. Ann Rev Biochem 61, 721–759.
Vasioukhin V (2006). Lethal giant puzzle of Lgl. Dev Neurosci 28, 13–24.
Vicente-Manzanares M, Choi CK, Horwitz AR (2009a). Integrins in cell migration—the actin connection. J Cell Sci 122, 199–206.
Vicente-Manzanares M, Koach MA, Whitmore L, Lamers ML, Horwitz AF (2008). Segregation and activation of myosin IIB creates a rear in migrating cells. J Cell Biol 183, 543–554.
Vicente-Manzanares M, Ma X, Adelstein RS, Horwitz AR (2009b). Non-muscle myosin II takes centre stage in cell adhesion and migration. Nat Rev Mol Cell Biol 10, 778–790.
Vicente-Manzanares M, Zareno J, Whitmore L, Choi CK, Horwitz AF (2007). Regulation of protrusion, adhesion dynamics, and polarity by myosins IIA and IIB in migrating cells. J Cell Biol 176, 573–580.
Webb DJ, Donais K, Whitmore LA, Thomas SM, Turner CE, Parsons JT, Horwitz AF (2004). FAK-Src signalling through paxillin, ERK and MLCK regulates adhesion disassembly. Nat Cell Biol 6, 154–161.
Zaidel-Bar R, Milo R, Kam Z, Geiger B (2007). A paxillin tyrosine phosphorylation switch regulates the assembly and form of cell-matrix adhesions. J Cell Sci 120, 137–148.